PRPD Construction and Analysis Using HFCT in Oil-Immersed High-Voltage Current Transformers

Kaynan Maresch*, Christoph Andres†, Martin Wolter†, Ghendy Cardoso Jr*, Aécio L. Oliveira*,
Luiz F. Freitas-Gutierres*, Marcus V. A. Nunes‡, Maurício Sperandio§
* Laboratory for Analysis and Protection of Electrical Systems, Federal University of Santa Maria, Santa Maria, Brazil
Emails: kaynan.maresch@acad.ufsm.br, ghendy@ufsm.br, aecio.oliveira@ufsm.br, luiz.gutierres@ufsm.br
†Institute of Electrical Power Systems, Otto von Guericke University Magdeburg, Magdeburg, Germany
Emails: christoph.andres@ovgu.de, martin.wolter@ovgu.de
‡High and Extra-High Voltage Laboratory, Federal University of Pará, Belém, Brazil
Email: mvan@ufpa.br
§Center of Excellence in Energy and Power Systems, Universidade Federal de Santa Maria, Santa Maria, Brazil
Email: mauricio.sperandio@ufsm.br

***Abstract*—This work investigates the evolution of partial discharge (PD) activity in oil-immersed current transformer under progressive oil removal. Electrical and electromagnetic measurements with high-frequency current transformers (HFCTs) were employed to detect and extract PD pulses. phase-resolved partial discharge (PRPD) patterns were constructed, taking into account the equivalent voltage phase angle for each pulse. Statistical parameters, including mean and peak values of charge and HFCT signal, were analyzed to quantify PD evolution. Results indicate negligible activity up to 5% oil loss, with significant discharges appearing beyond 7%, while HFCT-based measurements closely match electrical detection. The study demonstrates the effectiveness of PRPD analysis and HFCT sensors for non-invasive monitoring of insulation deterioration in high-voltage equipment.**

***Index Terms*—Current transformer, High frequency current transformer, Partial discharges, Phase resolved partial discharges.**

I. Introduction

Partial discharge (PD) is defined in [1] as a localized electrical discharge that only partially bridges the insulation between conductors and may or may not occur adjacent to a conductor. PD activity is a well-known indicator of insulation degradation in high-voltage (HV) equipment, and its accurate detection is fundamental to ensuring system reliability and preventing catastrophic failures. When a PD occurs, it can manifest in several ways: an electrical current flows, generating electromagnetic radiation; the movement of electrons and ions produces heat, causing pressure waves that result in audible or ultrasonic signals; excited atoms emit photons in the visible and ultraviolet ranges; and collisions with the surrounding medium may create identifiable chemical components [2].

Among the available detection techniques, the high-frequency current transformer (HFCT) stands out for its simplicity, broadband frequency response, and non-invasive installation. HFCT sensors detect the high-frequency components of PDs currents propagating through the ground or HV conductors. Typically wound on split ferrite cores with a response exceeding 30 MHz, HFCTs enable reliable PD pulse detection without interrupting equipment operation [3].

Recent studies have demonstrated the potential of HFCT-based monitoring for condition assessment of instrument transformers (IT) in field applications. In current transformers (CTs), most major failures result from internal dielectric breakdown, often initiated by insulation degradation due to PDs [4]. The work in [5] investigated the separation and classification of PD sources in substations, whereas [6] proposed a method for extracting PD pulses and constructing phase resolved partial discharge (PRPD) patterns in ITs and surge arresters. Nevertheless, the correlation between electrical and electromagnetic PD signatures under different insulation conditions, particularly in oil-immersed ITs, remains insufficiently explored.

In [7], a comprehensive study on the causes and types of IT failures is presented. The study shows that, among minor failures, 68.1% are related to sealing components (gaskets and O-rings), which, when compromised, can potentially lead to oil leakage in ITs. Motivated by these observations, the present work reports an experimental investigation of PD evolution in a 242 kV CT subjected to progressive oil removal.

The primary objective of this study is to construct PRPD patterns based on HFCT measurements, demonstrating that this approach allows non-invasive, online monitoring of the CTs in service. Since PRPD patterns are essentially built from the amplitudes of individual PD pulses and their corresponding phase angles, methodologies are proposed for peak detection of PD pulses in a noisy environment and for processing the voltage signal to determine the pulse occurrence angle in degrees. The measurements follow the procedures recommended by IEC 60270 [1], enabling a direct comparison between the PRPD patterns obtained from the HFCT and those from the conventional electrical method, which requires the CT to be de-energized. Another objective of this work is to demonstrate that oil loss may lead to critical conditions and that the proposed approach is capable of detecting this defect.

The present work was carried out with the support of the Coordination of Improvement of Higher Level Personnel - Brazil (CAPES/PROBRAL) - Process Number 88887.895158/2023-00.

979-8-3315-8138-1

II. Detection and extraction of PD pulses

The detection of PDs in high-frequency current signals requires methods capable of isolating short-duration transients in a noisy environment. In this work, a Discrete Wavelet Transform (DWT) [8] is used to suppress low-frequency noise and enhance high-frequency pulses, followed by a thresholding technique for peak detection.

A. Discrete Wavelet Decomposition

The DWT is a time-frequency analysis that decomposes a signal into multiple components corresponding to different frequency bands. The wavelet expansion of a signal $x(\theta)$ can be expressed as [9]:

$$x(\theta) = \sum_j \sum_k \alpha_{jk} f_{jk}(\theta), \tag{1}$$

where j and k are integers, $f_{jk}(\theta)$ are the wavelet basis functions, and α_{jk} are the corresponding expansion coefficients [9].

In this paper, the Reverse Biorthogonal wavelet family was selected with a fourth-level decomposition, since this wavelet type has demonstrated robust performance and high noise immunity across different signal conditions [10].

B. Threshold Definition

Being $D_4[n]$ denoted the reconstructed detail signal from level four of the wavelet decomposition. The detection threshold T is defined by:

$$T = \alpha \sigma_{D_4}, \tag{2}$$

where σ_{D4} is the standard derivation of $D_4[n]$ and $\alpha = 3$ an empirically chosen sensitivity factor. The thresholding α assumes that the noise follows an approximately Gaussian distribution centered around zero.

C. Pulse Localization

The pulse locations are determined by identifying the local maxima of the detail signal that exceed the threshold T:

$$\begin{cases} D_4[n_i] > T, & \text{detection threshold} \\ D_4[n_i] = \max\limits_{|n-n_i|<\Delta_{\min}} D_4[n], & \text{local maximum condition} \end{cases} \tag{3}$$

where Δ_{min} defines the minimum distance between consecutive detections, preventing false double-counting. The empirical value of $\Delta = 2\,\mu\text{s}$ is used. Ensure that closely spaced oscillations from a single discharge are grouped as one pulse. This step isolates the temporal positions of transient events, producing the discreet indices n_i that represent the occurrences of pulses of PD in the signal.

D. Pulse Window Extraction

Once the peak locations n_i are identified, short segments of the original discrete HFCT voltage signal $V_{\text{HFCT}}[n]$ with a sampling frequency of f_{s} are extracted around each detected peak. For each index n_i, a window of length N_{w} is defined, corresponding to a duration of $2\,\mu\text{s}$:

$$N_{\text{w}} = \text{round}(2 \times 10^{-6} f_{\text{s}}). \tag{4}$$

The extraction window is slightly asymmetric, including one-third of the samples before and two-thirds after the detected peak:

$$V^{(i)}_{\text{p-HFCT}}[n] = V_{\text{HFCT}}[n], \quad n \in \left[n_i - \tfrac{N_{\text{w}}}{3},\, n_i + \tfrac{2N_{\text{w}}}{3}\right]. \tag{5}$$

This asymmetry ensures that the discharge oscillations are fully captured within the extracted pulse. If a pulse occurs near the boundaries of the signal, zero-padding is applied to maintain a consistent window length across all extracted pulses. Using the original HFCT waveform, rather than the signal reconstructed from the wavelet detail, preserves both the amplitude and polarity of the pulses, at the cost of retaining background noise.

E. Amplitude Characterization

The dominant amplitude A_i of each extracted pulse is determined based on a condition variable C_i, defined as $C_i = 1$ if $|\max(V^{(i)}_{\text{p-HFCT}}[n])| > |\min(V^{(i)}_{\text{p-HFCT}}[n])|$, and $C_i = 0$ otherwise, as expressed in :

$$A_i = \begin{cases} \max(V^{(i)}_{\text{p-HFCT}}[n]), & \text{if } C_i = 1, \\ \min(V^{(i)}_{\text{p-HFCT}}[n]), & \text{if } C_i = 0. \end{cases} \tag{6}$$

This amplitude serves as a quantitative measure of pulse magnitude and is later used to construct the PRPD pattern.

III. Equivalent Voltage Angle Estimation

Accurate determination of the instantaneous voltage phase is essential for relating detected current pulses to the corresponding point in the voltage cycle. The voltage signal $V[n]$ measured simultaneously with the HFFCT signal was processed to obtain a continuous equivalent phase angle, detonated $\theta_{\text{eq}}[n]$, representing the instantaneous position of the fundamental component of the voltage waveform. The method is based on the Fourier analysis of a sliding window.

A. Filtering and Resampling

The raw voltage signal, measured with an oscilloscope, is smoothed and resampled to simplify computation and suppress high-frequency noise. A moving average filter of length $N = 10^5$ samples is used as:

$$V_{\text{filt}}[n] = \frac{1}{N} \sum_{k=n-\frac{N}{2}}^{n+\frac{N}{2}} V[k]. \tag{7}$$

979-8-3315-8138-1

Since the sampling frequency f_s is very high (to capture the high frequency pulses), the smoothed voltage is resampled to a lower rate $f_s^{'} = 10\,\text{kHz}$, maintaining the fundamental component near to $60\,\text{Hz}$.

B. Sliding Fourier Window

The equivalent voltage angle is derived from a local estimation of the fundamental component using a sliding Discrete Fourier Transform (DFT), implemented through a finite window of N_{cycle} samples corresponding to one electrical period, defined by $N_{\text{cycle}} = f_s^{'}/f_0$, where $f_0 = 60\,\text{Hz}$ is the nominal fundamental frequency.

The local cosine and sine components of the signal within each window are computed as:

$$Y_c[i] = \frac{2}{N_{\text{cycle}}} \sum_{n=0}^{N_{\text{cycle}}-1} V'[i+n] \cos\left(\frac{2\pi f_0 n}{f_s'}\right), \tag{8}$$

$$Y_s[i] = -\frac{2}{N_{\text{cycle}}} \sum_{n=0}^{N_{\text{cycle}}-1} V'[i+n] \sin\left(\frac{2\pi f_0 n}{f_s'}\right). \tag{9}$$

This computation corresponds to a discrete correlation between the voltage signal and reference sinusoids at the fundamental system frequency. The coefficients $Y_c[i]$ and $Y_s[i]$ form the real and imaginary parts of the complex phasor representation as:

$$\underline{Z}[i] = Y_c[i] + \mathrm{j}\, Y_s[i]. \tag{10}$$

C. Phasor Magnitude Phase Angle

The instantaneous amplitude and phase of the fundamental voltage component are obtained with:

$$|\underline{Z}[i]| = \sqrt{Y_c[i]^2 + Y_s[i]^2}, \tag{11}$$

$$\theta_V[i] = \tan^{-1} \frac{Y_s[i]}{Y_c[i]} \frac{180}{\pi}. \tag{12}$$

The $|\underline{Z}[i]|$ represents the local peak amplitude of the voltage waveform and $\theta_V[i]$ gives the instantaneous phase angle in degrees.

D. Phase Reference and Angle Correction

To eliminate the influence of phase delays introduced by filtering and windowing, the same Fourier procedure is applied to a synthetic reference cosine $r[n] = \cos(2\pi f_0 n/f_s^{'})$. The reference angle $\theta_{\text{ref}}[i]$ is obtained in the same manner as $\theta_V[i]$, and the final equivalent angle is computed as:

$$\theta_{\text{eq}} = \theta_V - \theta_{\text{ref}}[i]. \tag{13}$$

To align with experimental conventions, a constant of $+90^o$ is added and the operation (14) guarantees that the equivalent equivalent phase varies between 0^o and 360^o:

$$\theta_{\text{eq}}[i] = \text{mod}(\theta_{\text{eq}}[i] + 90^\circ,\, 360^\circ)\,. \tag{14}$$

E. Validation of the Proposed Methodology

For validation, a signal from a saline pollution test on a $145\,\text{kV}$ IT (ESDD $\approx 0.05\,\text{mg}\,\text{cm}^{-2}$, $79.7\,\text{kV}$) was used. Fig. 1 shows a the signal acquired in the laboratory, including the voltage from the capacitive divider ($V[n]$) and the HFCT signal from the equipment grounding terminal ($V_{\text{HFCT}}[n]$). Using the procedures described in Sections II and III, the raw data were processed to obtain the electromagnetic PRPD (Fig. 2). Comparing the obtained results with the reference diagram (Fig. 3), obtained using the electrical method, it is possible to observe that both diagrams exhibit strong similarity in phase distribution and pulse morphology. This confirms that the electromagnetic signal accurately reproduces the discharge activity detected by the conventional electrical measurement. Minor differences are mainly attributed to the acquisition duration: the electrical PRPD was recorded over $15\,\text{s}$, whereas the electromagnetic measurement, sampled at $100\,\text{MHz}$, covers only a few cycles, resulting in fewer detected pulses.

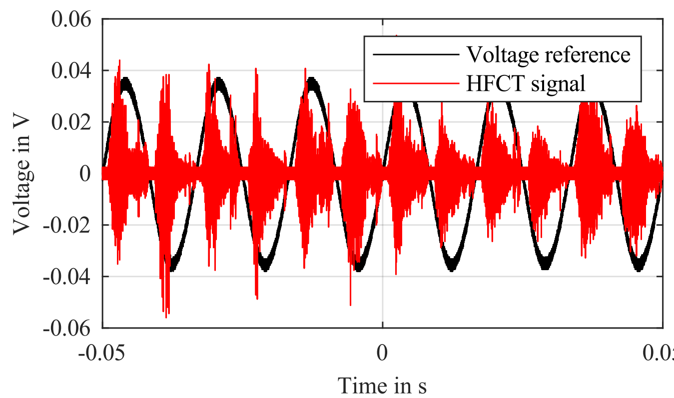

Fig. 1. Voltage reference and HFCT signal.

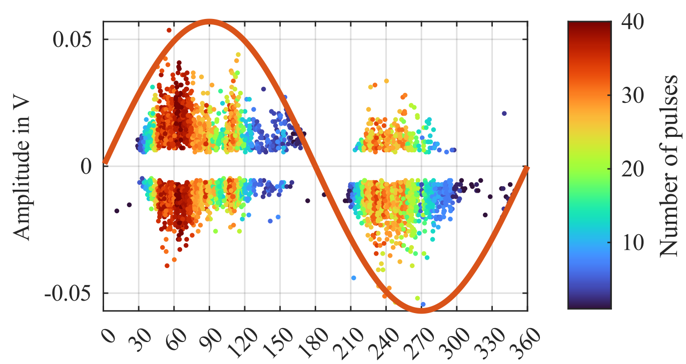

Fig. 2. Method validation, electromagnetic PRPD.

The cross-correlation between the phase histograms of the electrical and HFCT methods yielded $r = 0.42$, indicating a moderate agreement. This suggests that, although the match is not perfect, the HFCT is able to reproduce the main regions of pulse concentration observed with the electrical method, as can be seen in Fig. 4.

979-8-3315-8138-1

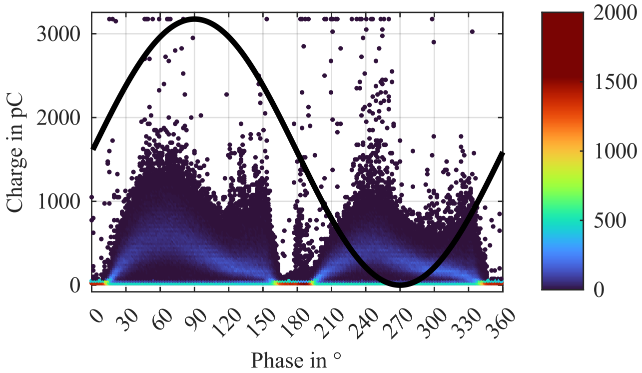

Fig. 3. Method validation, electric PRPD.

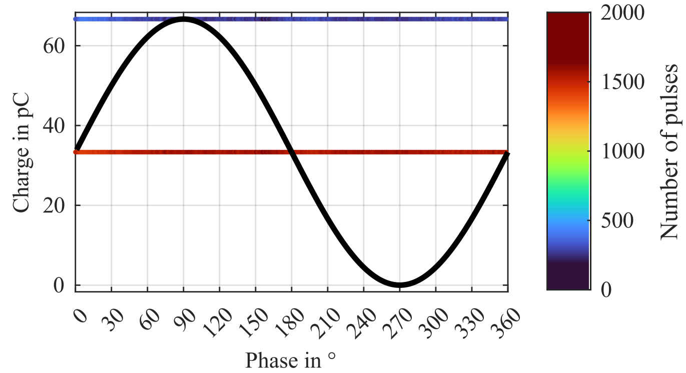

Fig. 5. Measurement 1 under normal condition: electric PRPD.

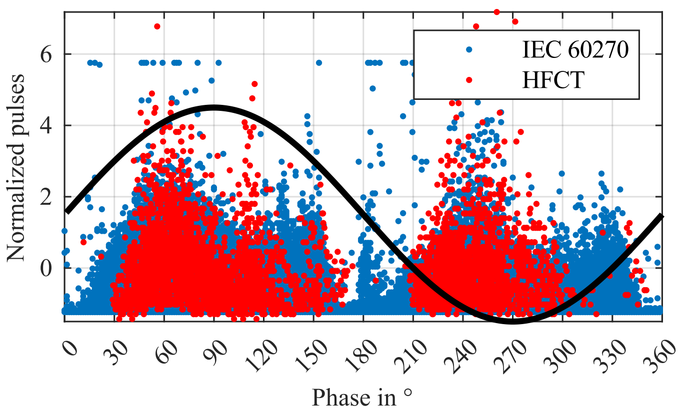

Fig. 4. Comparison between electric and electromagnetic PRPD.

IV. Performed Tests

A. Overview of Test Conditions

The experimental tests were conducted in a controlled laboratory environment, where different oil levels were removed from the $242\,\mathrm{kV}$ CT to simulate varying insulation conditions. The total weight of the insulation oil in the CT is $91\,\mathrm{kg}$, according to the information provided on the equipment's plate. PDs measurements were then performed under nominal voltage $(132.8\,\mathrm{kV})$.

For the conventional electrical method, a DDX 9121 ARIV PD detector was employed. In parallel, electromagnetic measurements were carried out using a HFCT with a bandwidth of $1\,\mathrm{MHz}$ to $80\,\mathrm{MHz}$ [11], installed in the grounding connection of the equipment. The voltage reference was obtained from a capacitive divider. Both signals, from the HFCT and the capacitive voltage divider, were simultaneously acquired using a digital oscilloscope with a $350\,\mathrm{MHz}$ analog bandwidth and $2.5\,\mathrm{GHz/s}$ sampling rate.

A total of seven oil extractions were performed, corresponding to 1% $(910\,\mathrm{g})$, 2% $(1820\,\mathrm{g})$, 3% $(2730\,\mathrm{g})$, 4.18% $(3800\,\mathrm{g})$, 5% $(4700\,\mathrm{g})$, 7.14% $(6520\,\mathrm{g})$, and 10.19% $(9270\,\mathrm{g})$.

B. Electrical and Electromagnetic PRPD Comparison

Under nominal conditions, both the electrical and electromagnetic methods exhibit only background noise, showing no phase correlation. This pattern remained practically unchanged up to an oil removal of 10.19%.

When the oil level is reduced by approximately 10%, distinct discharge clusters appear, distributed along the voltage phase. The PRPD obtained from the HFCT reproduces the same phase-resolved pattern observed in the electrical method, confirming that the electromagnetic signal preserves the temporal and polarity characteristics of the PD pulses, but with lower amplitude.

For measurement 8, corresponding to 10% oil removal, the nominal voltage could not be applied. Instead, a reduced voltage of $90\,\mathrm{kV}$ was used due to the high PD activity as evidenced by the electromagnetic PRPD (Fig. 6) and electrical PRPD (Fig. 7). Nevertheless, inspection of the PRPD patterns reveals that both methods present phase distributions consistent with internal PDs, characterized by pulse occurrence near the voltage zero-crossing [2]. This phase correlation confirms that the HFCT sensor captured the same discharge phenomenon observed by the conventional electrical measurement.

C. Statistical Analysis and Discussion

A statistical analysis of the detected pulses was performed to quantify the PD evolution. Table I summarizes representative parameters extracted from the electromagnetic and electrical PRPD data. While the first six measurements exhibit low mean and peak values, a marked increase occurs after oil removal exceeds approximately 7%, indicating the onset of internal PDs. It should be noted that the weak PD indication observed in Measurement 7 is very subtle and borderline, although detectable, it is not as the clear activity recorded in Measurement 8. The recurring values of $50\,\mathrm{pC}$ (mean charge) and $66.67\,\mathrm{pC}$ (max charge) in most tests are likely influenced by laboratory background noise.

The electrical method clearly indicates a sharp increase in discharge magnitude for Measurement 8, with mean and maximum charge values rising substantially, confirming the onset of intense PD activity. By contrast, the electromagnetic method shows lower variation in the statistical values.

The results further demonstrate that PD activity becomes significant only after substantial oil removal, showing that the insulating medium preserves its dielectric integrity up to

979-8-3315-8138-1

roughly 5% oil loss. When the oil level reaches approximately 7%, conductive regions of the winding or terminals become partially exposed. In this condition, the local electric field can intensify in the exposed regions, promoting the occurrence of partial discharges. Thus, the onset of PDs is directly related to the reduction of liquid insulation and the consequent alteration of the electric field distribution.

TABLE I
REPRESENTATIVE STATISTICAL PARAMETERS FROM PRPD DATA

M	Oil removal in %	Mean charge in pC	Max charge in pC	Mean V_{HFCT} in V	Max V_{HFCT} in V
1	0.0	50.00	66.67	1.67E-5	0.0044
2	1.0	54.37	100	7.62E-5	0.0320
3	2.0	50.00	66.67	5.45E-5	0.0100
4	3.0	50.00	66.67	7.65E-5	0.0140
5	4.18	50.00	66.67	2.66E-5	0.0080
6	5.0	50.00	66.67	-6.46E-5	0.0072
7	7.1	58.78	100	-1.76E-6	8.0E-5
8	10.2	3730.40	13387	-1.20E-4	0.0042

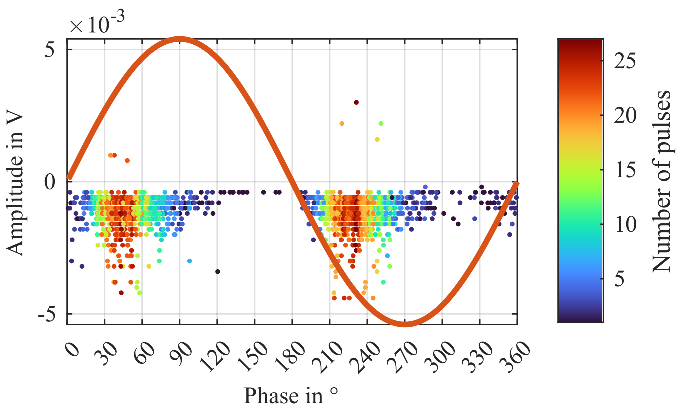

Fig. 6. Measurement 8 with 10.2% oil removal: electromagnetic PRPD.

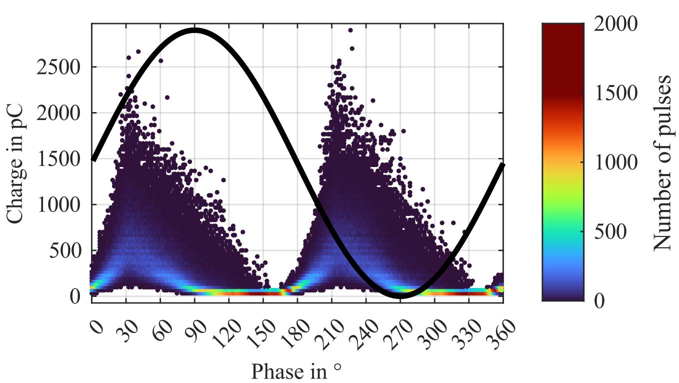

Fig. 7. Measurement 8 with 10.2% oil removal: electric PRPD.

V. CONCLUSION

The results confirm the feasibility of using the HFCT sensor to detect PD activity in oil-immersed CTs, with both electrical and electromagnetic measurements showing consistent PRPD patterns. However, the relatively large oil removal in this study likely accelerated the onset of discharges; future tests with smaller, controlled reductions could help characterize the early stages of internal PDs development.

From an application standpoint, HFCT-based monitoring shows strong potential for in-field detection of PDs due to its non-invasive installation and broadband response. Nevertheless, certain limitations must be addressed. The high electromagnetic noise typically present in substations may mask weak PD signals, and the need for a synchronized voltage reference poses practical challenges. Possible alternatives include the use of a Rogowski coil on the CT secondary circuit or a leakage-current detector, as used in [5].

Overall, the experimental methodology proposed here effectively reproduces internal discharge behavior and yields PRPD patterns characteristic of insulation degradation. These results highlight the HFCT as a promising tool for condition assessment and diagnostic studies of CTs under field conditions.

REFERENCES

[1] "High-voltage test techniques – partial discharge measurements," 2015. IEC Standard 60270:2015.
[2] G. C. Stone, A. Cavallini, G. Behrmann, and C. A. Serafino, *Practical partial discharge measurement on electrical equipment*. John Wiley & Sons, 2023.
[3] G. Stone, "Partial discharge diagnostics and electrical equipment insulation condition assessment," *IEEE Transactions on Dielectrics and Electrical Insulation*, vol. 12, no. 5, pp. 891–904, 2005.
[4] S. Asefi, B. Asad, M. Leinakse, H. Manninen, J. Kilter, T. Vaimann, A. Kallaste, M. Tealane, and M. Landsberg, "Review of high-voltage instrument transformer condition monitoring," *IEEE Transactions on Dielectrics and Electrical Insulation*, vol. 31, no. 6, pp. 3331–3341, 2024.
[5] J. V. J. Melo, G. R. S. Lira, E. G. Costa, P. B. Vilar, F. L. M. Andrade, A. C. F. Marotti, A. I. Costa, A. F. Leite Neto, and A. C. d. Santos Júnior, "Separation and classification of partial discharge sources in substations," *Energies*, vol. 17, no. 15, 2024.
[6] M. A. d. A. Romano, A. M. de Morais, M. V. A. Nunes, K. Maresch, L. F. Freitas-Gutierres, G. Cardoso, A. d. L. Oliveira, E. F. Martins, C. H. Correa, and H. C. Fontoura, "A novel method for online diagnostic analysis of partial discharge in instrument transformers and surge arresters from the correlation of hfct and iec methods," *Energies*, vol. 17, no. 19, 2024.
[7] A. Carvalho, M. L. Cormenzana, H. Furuta, W. Grieshaber, A. Hyrczak, D. Kopejtkova, J. G. Krone, M. Kudoke, D. Makareinis, J. Martins, K. Metrović, I. Ohno, J. L. Östlund, K.-Y. Park, J. Patel, C. Protze, M. Runde, J. Schmid, J. E. Skog, C. E. Sölver, B. Sweeney, and F. Waite, "Cigré technical brochure no. 512: Final report of the 2004 – 2007 international enquiry on reliability of high voltage equipment, part 4 - instrument transformers," 2012.
[8] I. Shim, J. Soraghan, and W. Siew, "Digital signal processing applied to the detection of partial discharge: an overview," *IEEE Electrical Insulation Magazine*, vol. 16, no. 3, pp. 6–12, 2000.
[9] S. M. Alessio, *Discrete Wavelet Transform (DWT)*, pp. 645–714. Cham: Springer International Publishing, 2016.
[10] M. A. Sahnoune, B. Zegnini, T. Seghier, A. Flah, M. Kanan, L. Prokop, and C. Z. El-Bayeh, "Noise source effect on the quality of mother wavelet selection for partial discharge denoising," *IEEE Access*, vol. 12, pp. 132729–132743, 2024.
[11] Doble Engineering Company, "Hfct clamp – high frequency current transformer." https://www.doble.com/product/hfct-clamp/, 2024. Accessed: Oct. 23, 2025.